Cicada wing surface topography: an investigation into the bactericidal properties of nanostructural features

S.M. Kelleher[a], O. Habimana[b], J. Lawler[c], B. O' Reilly[a], S. Daniels[d], E. Casey[b] and A. Cowley[d†]*

[a] *Biomedical Diagnostics Institute, Dublin City University, Dublin 9, Ireland*
[b]*School of Chemical and Bioprocess Engineering, University College Dublin, Belfield, Dublin 4, Ireland*
[c]*School of Biotechnology, Dublin City University, Dublin 9, Ireland*
[d]*National Centre for Plasma Science and Technology, Dublin City University, Dublin 9, Ireland*
[†]*Present address: European Astronaut Centre, Linder Höhe, D-51147 Cologne, Germany*
**Corresponding author: susan.kelleher@dcu.ie*

Abstract

Recently, the surface of the wings of the *Psaltoda claripennis* cicada species has been shown to possess bactericidal properties and it has been suggested that the nanostructure present on the wings was responsible for the bacterial death. We have studied the surface-based nanostructure and bactericidal activity of the wings of three different cicadas (*Megapomponia intermedia, Ayuthia spectabile* and *Cryptotympana aguila*) in order to correlate the relationship between the observed surface topographical features and their bactericidal properties. Atomic Force Microscopy and Scanning Electron Microscopy performed in this study revealed that the tested wings species contained a highly uniform, nanopillar structure on the surface. The bactericidal properties of the cicada wings was investigated by assessing the viability of auto-fluorescent *Pseudomonas fluorescens* cells following static adhesion assays and targeted dead/live fluorescence staining through direct microscopic counting method. These experiments revealed a 20 to 25% bacterial surface coverage on all tested wings species, however significant bactericidal properties were observed in *M. intermedia* and *C. aguila* species as revealed by the high dead:live cell ratio on their surfaces. The combined results suggest a strong correlation between the bactericidal

properties of the wings and the scale of the nanotopography present on the different wing surfaces.

Keywords

Bactericidal, nanostructures, cicada, surface science, and topography.

1. Introduction

The presence of nanostructural features on a wide range of materials have been shown to possess extremely useful properties for the biomedical field and beyond, with a broad spectrum of favourable properties including super hydrophobicity,[1] self-cleaning,[2] anti-biofouling,[3] the ability to act as photonic crystals,[4] and antibacterial attributes.[5,6] In many applications, the key driver for the performance of these materials is directly attributed to the presence of nanostructured surfaces.

With the rising threat of acquired bacterial resistance to conventional bactericidal agents and drugs, the pursuit of efficient novel antibacterial approaches has gained momentum in recent years, especially within the scope of preventive antibacterial strategy of smart surface design.[7] Of the different novel strategic designs, surfaces capable of releasing antibiotics have shown to display effective bactericidal properties; however these have been shown to possess a number of disadvantages including long leaching times, lack of control of concentration upon delivery, and poor durability.[8-12] Consequently, an approach driven by a mechanism that is independent from existing conventional methods is of high importance, especially one based on the material's inherent properties, which would push new frontiers in antibacterial surface design. Hence, much attention has shifted to what the natural world has to offer by reverse-engineering bio-inspired antibacterial surface solutions. [13-15]

It is within the context of natural antibacterial surfaces that the presence of nanopillar surface structures on *Psaltoda claripennis* cicada wings was identified as having bactericidal properties against Gram-negative bacteria, which was attributed to a purely physical mechanism and not by any chemical attributes.[16] This was demonstrated by coating the cicada wings with a layer of gold and performing repeat cell studies; here it was shown that these chemically inert nanopillars also provided a bactericidal effect. It has been suggested that the adsorption of bacterial cell membrane onto the cicada wing surface lead to a stretching effect on the membrane, consequently leading to cell membrane rupture and death.[17,18] It has also been shown that Gram-positive bacteria, whose bacterial cell membrane is generally much thicker than that of Gram-negative bacteria, are not killed by this mechanism (Gram-negative bacteria contain a layer of peptidoglycan which is 2-3nm thick, whereas Gram-positive bacteria possess a thicker layer of 20-80nm).[19,20] . Bacterial adhesion is a very complicated process affected by many factors, such as bacterial properties, material properties and the environment. The surface hydrophobicity is particularly important in initial cell adhesion[21]; however, with lots of factors to take into account it can be difficult to study one factor in isolation. It is, however, well studied that superhydrophobic surfaces, that is surfaces which have a WCA of greater than 150^{o}, are antibiofouling i.e. cells in general do not adhere to these surfaces.[22-26] This is a result of reduced protein adsorption required for initial cell adhesion.[27] Hydrophobic surfaces (with a 90^{o}>WCA<150^{o}) are not generally antibiofouling and the level of bacterial adhesion to these surfaces depends greatly on other factors e.g. pH of the environment, hydrophobicity of the bacteria etc.[21] There is no direct correlation between the hydrophobicity/ hydrophilicity of a surface and any specific bactericidal effects, where cells are killed as a result of the surface wettability. The nanostructuring of surfaces with an ordered array of features increases the hydrophobicity as described by the Cassie and Wenzel models.[27] Depending on the material used and the scale of the nanostructure, these surfaces can display superhydrophobic or hydrophobic properties.

The role of different factors in cell adhesion to such surfaces is evident in the fact that Ivanova et. al. showed that the superhydrophobic cicada wings with which they worked (WCA 158^{o}) did enable cell adhesion; moreover, the surface was bactericidal as a result of the surface structure. However, given that researchers have shown that hydrophilic nanostructured black silicon (WCA 80^{o}) and nanostructured titanium (WCA 41^{o}) are also bactericidal, there is no trend observed regarding the wettability of these nanostructured materials and their bactericidal activity.[5,6] A greater understanding of the role of the surface topography on the antibacterial activity of such nanostructured materials could allow for the production of materials that represent a new bactericidal paradigm compared to traditional chemical based methods.

To date, the nanostructures across various cicada species have been studied for varying applications.[28-31] Sun et. al., have systematically investigated both the wetting and optical properties of different cicada species as a function of its structure.[32,33] Alongside studies on individual properties of cicada wings, researchers have begun to investigate the multifunctional aspects of such surfaces.[30,34,35] However, no systematic study of the role topography plays in the antibacterial activity of cicada wings has been carried out to date. A thorough understanding of the dimensions of the nanotopography relative to the bactericidal activity of these surface structures is vital if products possessing this antibacterial property are to be developed on a large scale. We were interested to see if this antibacterial property was a trait common to different cicada species and to what extent the different topographic dimensions affect any bactericidal activity. In this paper we report the analysis of the nanostructure and physical properties of three different species of cicada and the investigation into the antibacterial activity of each structure against the Gram-negative bacteria, *Pseudomonas fluorescens*.

2. Materials and Methods

2.1 Sample preparation

Three different species of dried, unmounted cicada were purchased online (insectartonline.com). The three species used in this work were 1) *Megapomponia intermedia* (**ME**), *2) Ayuthia spectabile* (**AY**) and *3) Cryptotympana aguila* (**CA**) (see **Figure 1**).

Figure 1 – *Images of cicada samples used in this study; from right to left: 1) M. intermedia (**ME**), 2) C. aguila (**CA**) and 3) A. spectabile (**AY**).*

For consistency, the upper forewing of all species was studied; this means that for the **ME**, **CA** and **AY** samples, the colourless part of the forewing was studied. Each wing showed the same nanopattern on both the dorsal and the ventral side of the wing. Wing samples were cut to the required size (~ 1cm^2) using sharp scissors, sonicated in deionised water (<18 M Ω, obtained from a MilliQ system from Millipore, Ireland) for 15 minutes and dried under a stream of nitrogen. It should be noted that sonication does not affect the surface structure of the nanopattern (**Figure S1** in the Supporting Information for SEM images of sonicated and non-sonicated wings). For contact angle measurements and atomic force microscopy, samples were immobilised onto clean microscope slides using "President light body" silicone-based elastomer (Coltene Whaledent, West Sussex, United Kingdom) when a small amount of uncured elastomer was deposited on the slides and the wing samples were placed gently on top using fine tweezers. The elastomer cured and solidified after five minutes in air at room temperature, immobilising the wings to the surface of the slide. The main benefit of this method was that the wings remained very stable for imaging but that they could be pulled off gently afterwards if required.

2.2 Contact angle measurements

Contact angle (CA) analysis was performed using an OCA 35 goniometer (Dataphysics). Droplets of 4µL of deionised water (<18 M Ω, obtained from a MilliQ system from Millipore, Ireland) or diiodomethane (Sigma Aldrich Ltd, Arklow, Ireland) were employed for CA analysis, at a dose rate of $1\mu Ls^{-1}$. The CAs of a minimum of three droplets were measured per sample. Surface energies were calculated using the measured CAs for water and diiodomethane on each surface using the Owens-Wendt-Rabel-Kaelble (OWRK) method and the Ström models for the solvents.[36-38] The OWRK is an extended version of the Fowkles equation for calculation surface free energy; it divides the surface free energy into a polar part and a disperse part, and includes the hydrogen-bonding interactions. This model requires the measurement of two or more liquids at the interface and in this is case, water (polar) and diiodomethane (dispersive) were used, and is a universal standard when measuring surface free energy of materials.[39]

2.3 Atomic force microscopy

Substrate surfaces were examined using an atomic force microscope (AFM) on a Veeco Dimension 3100 instrument. The AFM was used in tapping mode using Tap300Al-G tips from Budget Sensors (Sofia, Bulgaria) and high aspect ratio images were measured using Improved Super Cone tips from Team Nanotec (Villingen-Schwenningen, Germany). Both tips had a resonant frequency of 300 kHz and force constant of 40 Nm^{-1}. Images were analysed using WSxM software.[40]

2.4 Scanning electron microscopy

Scanning electron microscopy (SEM) images of the structures surfaces were taken using a Karl-Zeiss EVO series instrument. All samples were sputtered with a gold coating (~8 nm) using an Edwards Scancoat Six Sputter Coater prior to analysis under SEM. During sputtering, samples were immobilised onto glass substrates using the silicone elastomer to ensure they remained stable.

2.5 Statistical analysis of topography

The dimensions of the topography of the nanostructures were calculated out by analysis of both the AFM images (for accurate height measurements) and the SEM images (for accurate pitch and diameter measurements). For calculation of the average height, a minimum of three different images were taken and the average height was calculated using the histogram height distribution function in the WxSM software. High resolution SEM images were analysed in ImageJ, a Java-based image processing program (http://rsbweb.nih.gov/ij/), by converting to Binary and using the Feret Diameter measurement (for diameter) and centre-to-centre Nearest Neighbour Distance measurement (for pitch) in the Analyze Particles plug-in. A minimum of three images with over 100 structures were analysed for the pitch and diameter dimensions.

2.6 3D modelling

3D modelling of the wings was carried out using 3D computer-aided-design software, Solidworks. Models were produced based on the dimensions determined by SEM (diameter and pitch) and AFM measurements (height). The diameter of the top of the feature was deemed to be approximately half the base of the feature based on tilted SEM images. The angle of the incline of the protrusions was measured to be approximately 70^{o} from tilted SEM images.

2.7 Bacterial cell testing

The selected model bacterial strain for this study was a mCherry-expressing *Pseudomonas fluorescens* PCL1701. Cultures were obtained by inoculating 100 mL of raw water medium supplemented with gentamicin at a final concentration of 10 μg mL^{-1} using a single colony of a previously grown culture on King B agar (Sigma-Aldrich, Ireland) at 30°C. The inoculated medium was then incubated at 30 °C with shaking at 200 rpm and left to grow to an optical density (OD_{600}) of 0.4. Cell concentration was standardized for each adhesion experiment by diluting the growth cultures to an OD_{600} of 0.2 in 40mL of 0.1 M NaCl (Sigma-Aldrich, Ireland). Cells were then harvested by centrifugation at 5000 rpm for 10 min and the cell pellet re-suspended in 40mL 0.1 M NaCl, resulting in an inoculum of approximately 10^8 cells mL^{-1}.

Adhesion tests were carried out on all wing samples. The cicada wings were cut into small sections and immobilized on cover slips using 2 strips of double-sided tape separated by a distance of at least 5 mm from tape extremities. Once immobilized, coverslips holding individual cicada wings were carefully placed at the bottom of 6-well plates (polystyrene, Sarstedt). The bottom of one of the remaining empty wells was used as a hydrophobic surface control with no surface nanopattern (RMS of ~3nm).[41] Bacterial adhesion was initiated by adding 4 mL of a freshly prepared OD_{600} =0.2 *P. fluorescens* suspension in individual wells. Wells were then statically left to rest for 30 minutes at room temperature. To end the adhesion experiments, 4mL clean 0.1 M NaCl solution was added in individual wells, followed by a systematic removal of 4 mL volume of diluted bacterial suspension. This process was repeated three times for each well of the 6-well plate.

To assess the degree of cell structural damage, a volume of 1 μL of SYTOX Green (5 mM) (Invitrogen, Dublin, Ireland) was added to individual wells of the 6-well plates. SYTOX Green is a rapid acting, high-affinity nucleic acid stain that does not cross the membranes of

live cells and yet easily penetrates cells with compromised plasma membranes e.g. dead or injured cells. Stained wells were subsequently incubated at ambient temperature for 10 min in the dark prior to epi-fluorescence microscopy (Olympus BX51) using a 10X objective. Two images were acquired for every chosen observation field using U-MNG and U-MWB filter cubes for differentiating between fluorescent mCherry-tagged and SYTOX Green-stained *Pseudomonas* cells, respectively. Ten different fields of view were obtained at random points from each cicada wing coupon samples and control surfaces. Cell surface coverage (%) for mCherry-tagged (live) and SYTOX Green-stained cells (dead) was determined for each tested membrane using ImageJ software. The adhesion experiment was performed three times using independent *P. fluorescens* cultures.

To check whether cicada wings were already covered by any dead/injured organisms, an additional control experiment was performed in which the wing surfaces were stained with SYTOX Green, incubated at ambient temperature for 10 min in the dark prior and analysed through epi-fluorescence microscopy. Following epi-fluorescence microscopy, fouled cicada wing samples were chemically fixated and dehydrated in their respective wells. Submerged membrane samples were fixed by adding glutaraldehyde to a final concentration of 2.5% and left to incubate overnight. All samples were then rinsed with 0.1M NaCl solution then gradually dehydrated using increasing volumes of ethanol for 5 min intervals, until samples were submerged in 100% ethanol. The wells were then emptied and the wings were left to dry. These fixed samples were studied with both AFM and SEM.

3. Results and Discussion

3.1 Surface topography analysis

The nanotopography of the surface of the cicada wings was analysed using AFM and SEM. A brief analysis of each area of the wing showed that the topography varied depending on the area of the wing which was studied. In general, coloured parts of the wings have a

more pronounced structure than the clear/ colourless parts. In addition, it was seen that the tubular vein features on cicada wing samples also possessed nanostructures, often with larger microstructures (see **Figure S2** in the Supporting Information for sample SEM images). In order to determine any correlation between the scale of the topography and antibacterial activity, thorough analysis of the dimensions of the wings was required. As outlined in section 2, for consistency the upper forewing of all species was used for in-depth analysis and cell testing experiments. The SEM images showing the surface topography of this part of each species are provided in **Figures 2a-c** (for **ME**, **CA and AY** respectively) and show surface structure of hexagonally-packed, uniform pillars (see **Figure S3** in the Supporting Information for larger SEM images). Topographical analysis of the surface structure imaged showed that there was a large variance in the scale of the pillars between samples, with pitches (centre-to-centre distances) calculated to be in the range of 165 ± 8 to 251 ± 31 nm and diameters calculated to be in the range of 156 ± 29 to 207 ± 62 nm (**Table 1**).

AFM imaging was used to accurately calculate the average height of the protrusions and results showed a range between 182-241nm (**Table 1**). AFM height images were taken using both standard and high aspect ratio tips, and no difference between height measurements with these tips was observed. All histograms for the height measurements are shown in **Figures 2a-c**, and demonstrate a narrow height range for the ordered structures. In addition cross-section profiling of the nanostructures in **Figures2a-c** show the uniformity on the wing surface as well as the relative sharpness of the nanopillars.

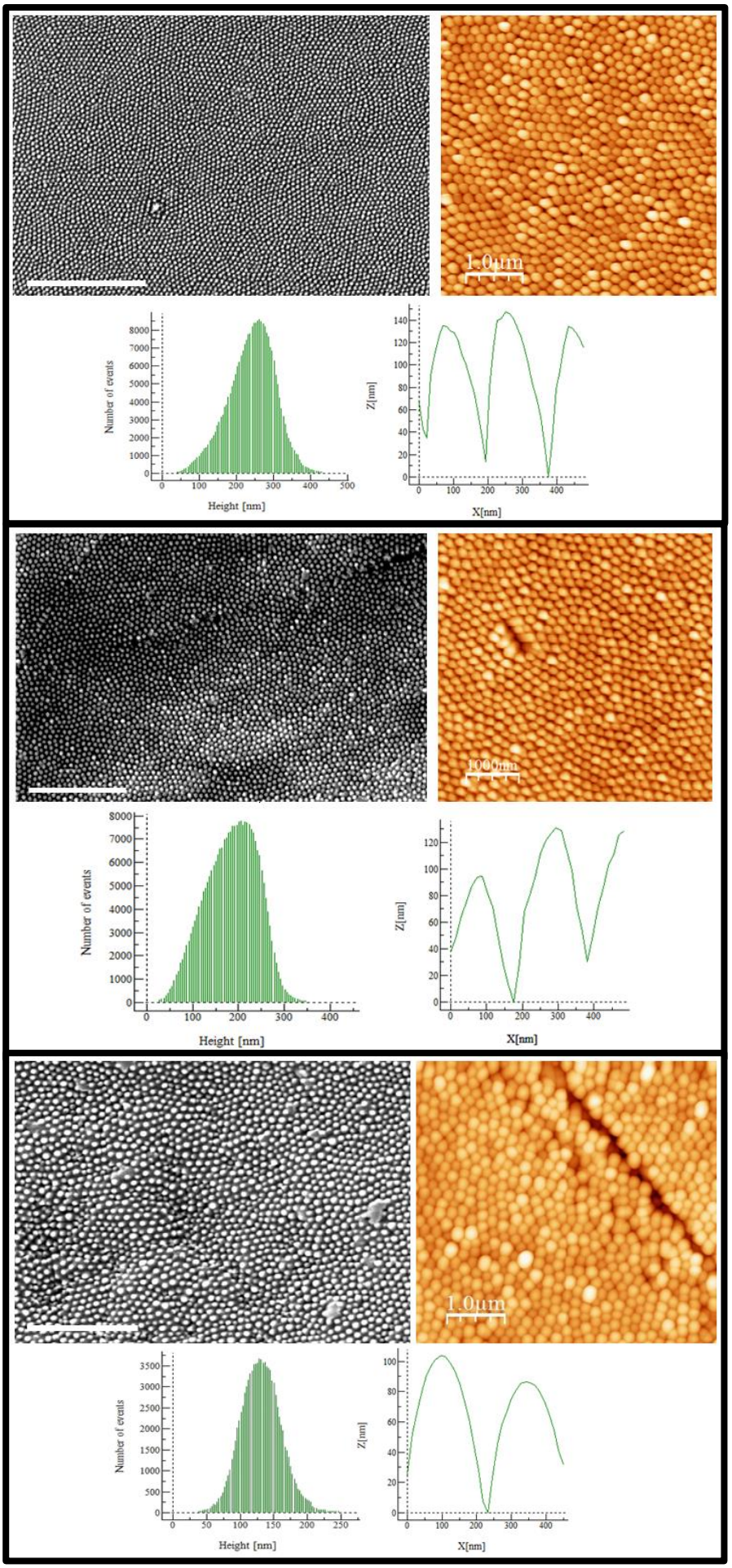
1.0μm
Number of events
Height [nm]
Z[nm]
X[nm]
1.0μm
Number of events
Height [nm]
Z[nm]
X[nm]
1.0μm
Number of events
Height [nm]
Z[nm]
X[nm]

Figure 2 - *SEM image, AFM height histogram, AFM height cross-section profile and AFM images (2D and 3D) of* ***a) ME****,* ***b) CA****, and* ***c) AY.*** *Scale bars in SEM images are all 4µm in length. AFM images are 5 µm x 5 µm. Profile images are all 500nm in the x direction.*

SEM images taken at a tilt of 30ºC showed that all species consisted of pillars which were tapered, terminating with a hemisphere top, with the observed diameter being approximately half the diameter of the base of the pillar; the average angle of incline for the protrusion from the surface was calculated to be 70º (between the pillar and the surface).

The average spacing (S) between protrusions was calculated by subtracting the average diameter from the average pitch (**Table 1**). The aspect ratio (height/diameter) of the **ME**, **CA,** and **AY** samples ranged from 0.88-1.55 (**Table 1**).

Wing	Height (H)	Pitch (P)	Diameter (D)	Spacing (S)	Aspect Ratio
ME	241	165 ± 8	156 ± 29	9	1.55
CA	182	187 ± 13	159 ± 47	28	1.15
AY	182	251 ± 31	207 ± 62	44	0.88

Table 1- *Average pillar height, pitch, diameter, spacing and aspect ratio for the different species of cicada wings. The values for H, P, D and S are in nanometres.*

3.2 Surface properties

The impact of hydrophilicity/hydrophobicity on the antibacterial properties of surfaces has been the topic of much research, in particular the influence on the adhesion of bacteria. Effective surfaces for the low adhesion of bacteria have been described as being hydrophilic, highly hydrated and non-charged.[42] However, super-hydrophobic materials (with a water contact angle of >150º) also have the potential to act as an antifouling material;[23] therefore, analysis of the water contact angle (WCA) of these materials is important when understanding the effect of bacterial adhesion to the surface. **Table 2** displays the measured WCA, contact angle from diiodomethane, the calculated surface energy, calculated solid fraction for the Cassie model (described below) and the roughness factor for the Wenzel

model (described below). All wings displayed high WCAs, with a range of 95.65 ± 9.01° to 135.5 ± 4.96° determined, demonstrating their hydrophobic nature.

Wing	WCA (deg)	I_2CH_2 CA (deg)	Surface Energy (mN/m)	φ (Solid fraction)	*r* (Roughness factor)
ME	135.5 ± 4.96	70.58 ± 10.08	25.25	0.89	6.46
CA	113.2 ± 4.59	68.6 ± 9.7	23.67	0.723	4.31
AY	95.65 ± 9.01	66.03 ± 11.11	26.85	0.68	3.4

Table 2 - *Water contact angles, contact angles from diiodomethane, calculated surface energy, solid fraction for the Cassie model and the roughness factor for the Wenzel model, for wing samples.*

There are two different models which describe the wetting of rough, nanostructured surfaces; the Wenzel model, where the liquid has completely penetrated into the nanostructures (called homogenous wetting) and the Cassie model[43], where there is air trapped under the liquid in the nanostructure (called heterogeneous wetting). These models are described by Equation 1 (Wenzel) and Equation 2 (Cassie) where θA is the apparent contact angle, r is the roughness factor, θo is Young's contact angle of a flat surface and ϕ is the fraction of solid material in contact with liquid.

$$\cos\theta A = r\cos\theta o \quad (1)$$

$$\cos\theta A = \phi(1 + \cos\theta o) - 1 \quad (2)$$

On a hydrophobic surface, the wetting is generally heterogeneous and is best described by the Cassie model where it is the reduction of the actual contact area of the solid–liquid that is responsible for increasing the hydrophobicity. As per the Wenzel model, the hydrophobicity is increased by increasing the roughness factor. The relationship between the topography and the wettability can be determined by relating the structure to the solid fraction in contact with the liquid (φ) for the Cassie model (Equation 3) as well as the roughness factor (r) (Equation 3) for the Wenzel model, where D = diameter, S = spacing,

and H = height of protusions.[24] **Figure 3a** shows the direct relationship between both of these factors calculated for the three wing samples (**Table 2**) and their WCAs. This trend is in agreement with previously published studies on the wettability of different cicada species.

$$r = \frac{(D+S)^2 + 4DH}{(D+S)^2} \quad (4)$$

Figure 3b shows the water droplet formed on a CA wing sample and the hydrophobic nature of the material can been seen. The contact angle of diiodomethane on each wing sample was measured in order to enable the calculation of the surface energy using the Owens-Wendt-Rabel-Kaelble model. This model is a universal standard for the calculation of surface free energy of surfaces and divides the energy into polar and dispersive parts, as well as including hydrogen-bonding interactions. For this reason, two liquid-solid interfaces are studied, one which has polar parts (e.g. water) and one which has dispersive parts (e.g. diioidomethane). As expected, the surface energy for all wing samples was low with a range of 23.67-26.85 mN/m. The surface free energy also plays a role on bacterial cell adhesion and several groups have investigated this in detail.[44-47] In particular, the free energy is one of the determining factors in long-range (>50 nm) interactions between cells and surfaces. Surface free energy and wettability are closely related and which possess a low surface energy ae often also hydrophobic, which can also be seen in **Table 2**; however, no direct relationship is observed, primarily likely due to the fact that several different factors are involved in both wettability and surface energy e.g. surface charge.[21] It has been previously reported that surfaces where the free energy was between 23 and 30 mN/m was related to the lowest bacterial adhesion, thus the potential for these surface to be antibiofouling (i.e. not promote the formation of a biofilm) was possible.[46]

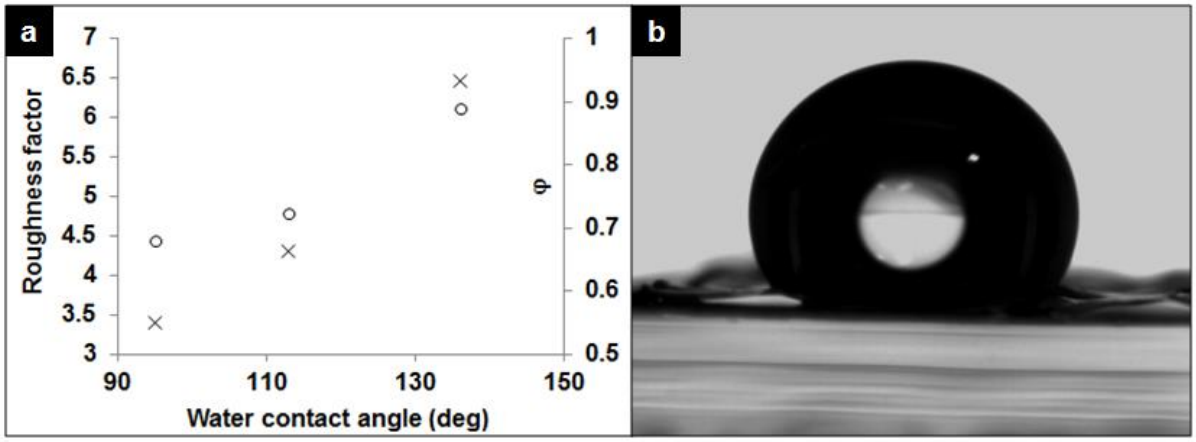

Figure 3 - *a)* *Graph showing the relationship between the WCA and both the roughness factor, r (corresponding to the Wenzel model) and the solid fraction in contact with the liquid,φ (for the Cassie model);* ***b)*** *Image of a 2µL droplet of water on the CA wing as seen with the WCA instrumentation.*

3.3 Bacterial cell testing

Wing samples were prepared for bacterial cell adhesion tests using a mCherry-expressing *P. fluorescens* strain. This bacterial strain was purposely chosen for its auto-fluorescence properties as well as for its classification as Gram-negative, which was demonstrated as having distinct sensitivity towards nanostructures present on specific cicada wing samples.[16] After 30 minutes, static adhesion experiments revealed a 20 to 25% bacterial surface coverage of *P. fluorescens* on all species, (**Figure 4a**). .

Subsequent staining of adhered cells with SYTOX Green for quantifying dead or injured cells revealed that the **AY** wing sample exhibited the same level of SYTOX Green positive cells as the control surface with on average 1.5% in surface coverage (**Figure 4b**). The **ME** and **CA** wing samples exhibited higher levels of dead or injured cells on their surfaces. **CA** exhibited double the amount of SYTOX Green positive cells compared to the control surfaces, whereas **ME** cicada wings had the highest level of dead cells; three times higher than the control (**Figure 4b**). The ratio of SYTOX Green-stained dead/injured to mCherry-expressing live cells on the difference surfaces confirmed the bactericidal effect of **CA** and **ME** cicada wings (**Figure 4c**). **CA** exhibited higher dead-cell ratios on its surface

compared to the control (p=0.0173). **ME** also showed higher dead-cell ratios when compared to the hydrophobic control (p<0.0001) and **CA** surfaces (p<0.0001). **Figure 4d** shows the fluorescent micrographs of the wings, showing the mCherry-expressing bacteria (live) and the SYTOX Green stained bacteria (dead). It can be seen that there is a greater number of dead cells on the **ME** and **CA** wings when compared to the **AY** sample. It should also be noted that no dead/injured cells were observed on the any of the cicada wings when stained with SYTOX Green prior to adhesion experiments, hence proving that the wings were clean of any potential dead cells, which could have led to a degree of bias in obtained results.

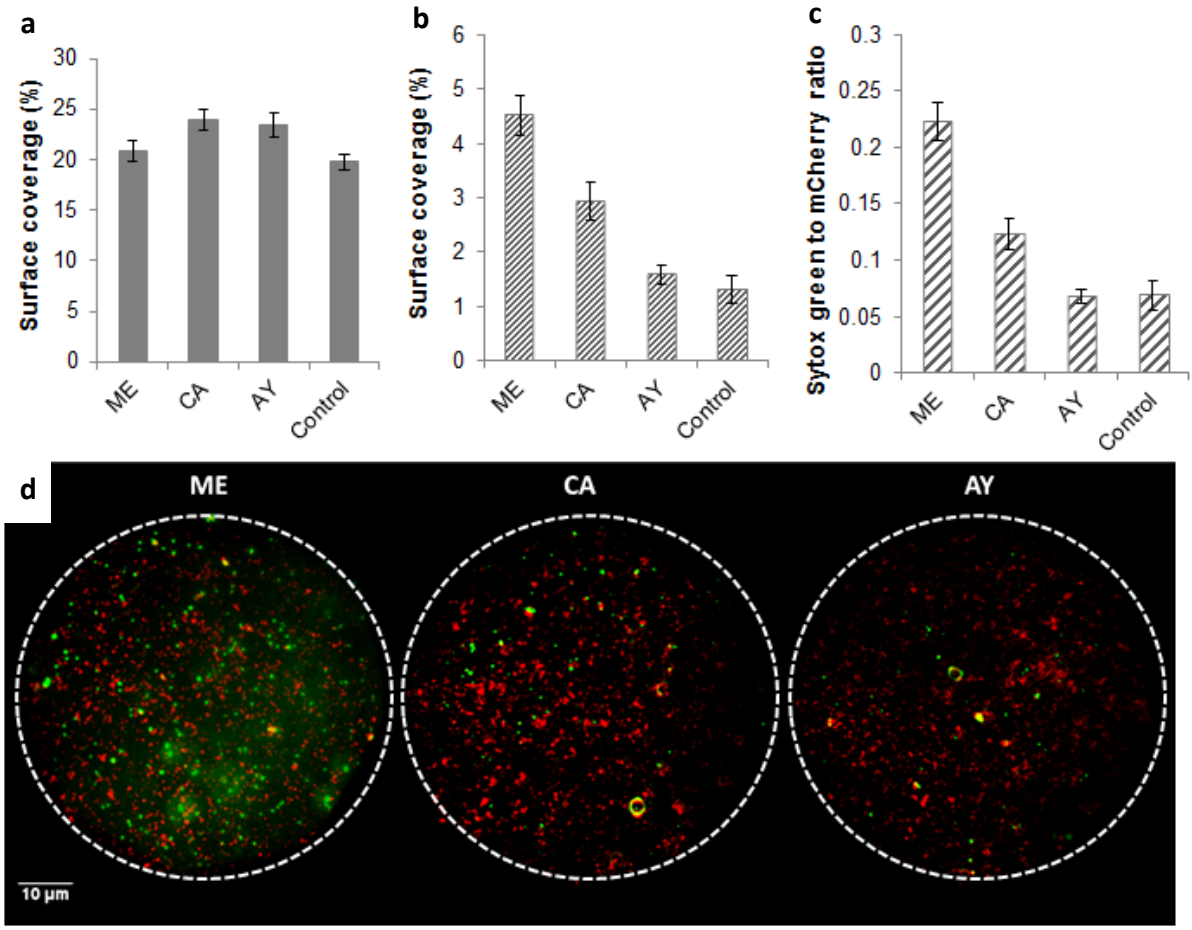

Figure 4 – *a)* *Surface coverage of mCherry expressing P. fluorescens after 30 minutes contact;* ***b)*** *Surface coverage of SYTOX Green stained P. fluorescens after dead/live staining of bacterial cells;* ***c)*** *Ratio of mCherry:SYTOX Green fluorescent signals after dead/live staining of bacterial cells;* ***d)*** *Fluorescent micrographs showing the dead/injured (green) and undamaged (red) cells.*

3.4 Surface analysis after bacterial cell testing

Adhered bacterial cell samples were fixated as described in section 2.7, gold-coated and imaged using SEM and AFM. The SEM images (**Figure 5a, c, e** and **g**) give an overview of the morphology of the bacteria on the surface. Cell surface coverage was found to be within the range previously described in the epi-fluorescence microscopy results and cells were found to be individually dispersed across **ME**, **CA** and **AY** wing samples (**Figure 5a, c,** and **e** respectively). *Pseudomonas* cells were observed to interact strongly with the nanostructure, pulling on the pillars and at times collapsing around the structure.

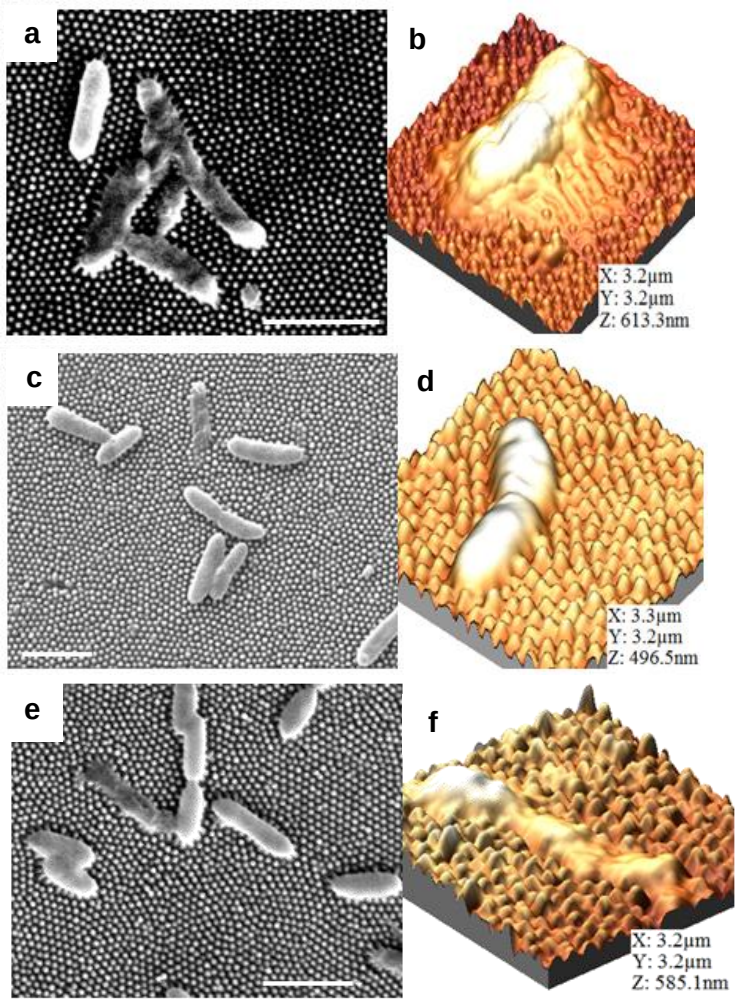

Figure 5 – *SEM images of fixed bacterial cells on **a) ME**, **c) CA** and **e) AY** wings. Scale bars on SEM images are 2µm in length; AFM images of bacterium on **b) ME**, **d) CA**, and **f) AY** wings. All AFM images are 3.2x3.2µm.*

AFM data offered a complementary qualitative dimension concerning the nature of this interaction (**Figure 5b, d,** and **f** respectively for **ME**, **CA,** and **AY**) with varying extents

of indentation seen by the nanopillars into the cells. This bacterial cell testing showed a strong bactericidal effect from the **ME** and **CA** wings against the Gram-negative *P. fluorescens,* for which there is strong evidence that the nanostructure plays a major role in this interaction.[5,16,19] In order to better understand the level of interaction between the nanostructure present on the various wings and bacterial cells, 3D models of each of the wings which have a periodic, uniform structure were prepared using the dimensions from **Table 1**. **Figure 6** shows the 3D models of the nanostructures and how they interact with a model bacterium of the average size of that which was used in our cell testing. We believe there is a correlation between the number of pillars the bacteria interact with and the bactericidal activity of the surface. It can be seen from the images that the **ME** and **CA** wings (**Figure 6a/6d** and **Figure 6b/6e** respectively) have tighter packing and smaller feature size when compared to the **AY** wings (**Figure 6c/f**).

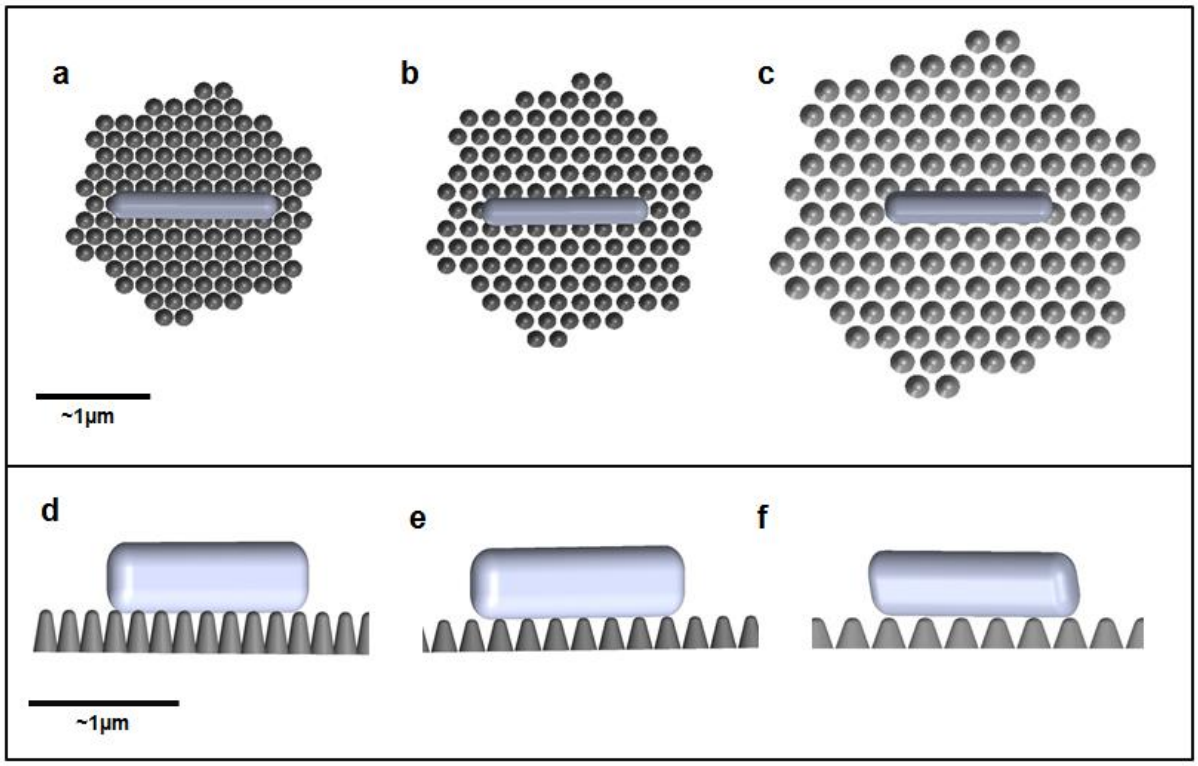

Figure 6 – *Birds-eye views of model bacterium on model **a) ME**, **b) CA**, and **c) AY** wing surfaces; side on profile views of the model bacterium on model **d) ME**, **e) CA**, and **f) AY** wing surfaces.*

Based on these models, surface area analysis (see **Table S1** in the Supporting Information for data) can provide an understanding of the level of interaction between an average bacterial cell and the different nanostructures. The area an average bacteria covers can be calculated as 574,000 nm^2 based on the average width and length of one bacterial cell, measured by AFM. Each sample can be described as being made up a hexagonal unit cell, centred on one pillar, the area of which can also be calculated using the measured pitch and diameter. This enables the calculation of the average number of unit cells, and therefore, the average number of pillars into which one cell interacts. This was calculated to be 24 for **ME**, 19 for **CA** and 10 for **AY**. The bacterial dead:live ratio for **ME**, **CA** and **AY** respectively is 0.222, 0.123 and 0.067. This correlation seems to suggest that the greater number of nanostructures with which these bacterial cells come into contact, the greater the bactericidal activity of the nanostructure; this could also be linked to the smaller the pitch and diameter of these features. The topography scale and bactericidal activity observed in this study is in line with the scale of previous work carried out on cicada wings, where the dimensions were: height = 200nm, pitch = 170nm and diameter = 60nm; here, one *P. aeruginosa* bacterium is observed to interact with between 20-30 nanopillars (as seen from published SEM images).[16] The cell membrane of the Gram-negative bacterium has been described as rupturing as a result of stretching between these tightly-packed pillars.[17]

This corroborates well with the findings of Nowlin et. al. where they investigated the fungicidal properties of two nanostructured cicada wings and a dragonfly wing.[18] Their experimental results indicate that the cell death is dependent upon morphology of the nanostructured surface and cellular surface adhesion strength, however even their weakest adhering strain of *Saccharomyces cerevisiae* used in their experiments experienced cell death when exposed to their smallest nanopillar diameters. This also coincides a recent model from F. Xue et. al. [20] whereby smaller, sharper nanopillars is shown to be a key factor in giving rise to much greater stretching to bacteria resting on them. Their calculations do not appear to

account for variations in the cell adhesion strength that Nowlin et. al. have experimentally shown, but do corroborate with the results experimentally described in this paper; although not quantitative, the AFM cross-sectional profiles shown in **Figure 2** as well as 3D AFM images (see **Figure S4** in the Supporting Information) show that there is an increase in the sharpness of the nanopillars from the **AY** to **CA** to **ME**, directly relating to their bactericidal activity. It can be therefore understood why this phenomenon of greater bactericidal activity is observed when greater numbers of nanopillars come into contact with the bacterial cell.

While the WCA of the wings correlates with the increase in the ratio of live:dead cells, there is no distinct correlation between the hydrophobicity of the wings and the bacterial surface coverage found on the wings. In addition, hydrophilic nanostructured surfaces have been shown to possess antibacterial properties, and as such it is likely that the role of the contact angle in the bactericidal properties of the wings is of little importance in relation to the dimensions of the nanostructures themselves.

Conclusion

We have carried out detailed characterisation of the topography of three different species of cicada wings using SEM and AFM imaging. The nanotopography was seen to vary depending on the species and often depending on the area of the wing which was studied. The wettability and surface energy of the wings was measured showing that the dimensions of the nanostructure are directly responsible for the hydrophobic characteristics and low surface energies of the wings. The bactericidal activity of the three species was studied by static adhesion tests and using SYTOX Green staining to identify the number of dead/injured cells; these experiments showed that two species, *Megapomponia intermedia* and *Cryptotympana aguila*, were active at killing *Pseudomonas fluorescens*, a Gram-negative bacterium, when compared to a hydrophobic control surface with no surface nanostructure. The correlation between the scale of the nanopillar structure and the level of bactericidal activity of these

surfaces has been demonstrated. We are currently conducting further experiments to study the bactericidal activity of the wings of the *Megapomponia intermedia* and *Cryptotympana aguila* species over longer periods of time in order to analyse whether or not these nanostructures have the ability to prevent biofilm formation.

Supporting Information

The following information is available in the Supporting information: **Figure S1 –** SEM images of **ME** before and after sonication; **Figure S2 –** Variance in nanotopography across **ME**; **Figure S3 –** SEM images of **ME, CA** and **AY**; **Figure S4 –** 3D AFM images of **AY, CA** and **ME**; **Table S1 –** Data used to calculate the average number of pillars per bacterial cell.

Acknowledgments

The presented work was supported by Science Foundation Ireland under grant numbers 13/TIDA/B2697 and 14/TIDA/2369, and the European Research Council (ERC), Project 278530, funded under the EU Framework Programme.

References

1. Bechert, D. W.; Bruse, M.; Hage, W. Experiments with Three-Dimensional Riblets as an Idealized Model of Shark Skin. Exp. Fluids 2000, 28, 403-412.

2. Gant, R. M.; Hou, Y.; Grunlan, M. A.; Cote, G. L. Development of a Self-Cleaning Sensor Membrane for Implantable Biosensors. J. Biomed. Mater. Res., Part A. 2009, 90A, 695-701.

3. Chung, K. K.; Schumacher, J. F.; Sampson, E. M.; Burne, R. A.; Antonelli, P. J.; Brennana, A. B. Impact of Engineered Surface Microtopography on Biofilm Formation of Staphylococcus Aureus. Biointerphases 2007, 2, 89-94.

4. Poborchii, V. V.; Tada, T.; Kanayama, T. A Visible-Near Infrared Range Photonic Crystal Made up of Si Nanopillars. Appl. Phys. Lett. 1999, 75, 3276-3278.

5. Ivanova, E. P.; Hasan, J.; Webb, H. K.; Gervinskas, G.; Juodkazis, S.; Vi Khanh Truong; Wu, A. H. F.; Lamb, R. N.; Baulin, V. A.; Watson, G. S.; Watson, J. A.; Mainwaring, D. E.; Crawford, R. J. Bactericidal Activity of Black Silicon. Nat. Comm. 2013, 4, 2838.

6. Sengstock, C.; Lopian, M.; Motemani, Y.; Borgmann, A.; Khare, C.; Buenconsejo, P. J. S.; Schildhauer, T. A.; Ludwig, A.; Koeller, M. Structure-Related Antibacterial Activity of a Titanium Nanostructured Surface Fabricated by Glancing Angle Sputter Deposition. Nanotechnology 2014, 25, 195101.

7. Bush, K.; Courvalin, P.; Dantas, G.; Davies, J.; Eisenstein, B.; Huovinen, P.; Jacoby, G. A.; Kishony, R.; Kreiswirth, B. N.; Kutter, E.; Lerner, S. A.; Levy, S.; Lewis, K.; Lomovskaya, O.; Miller, J. H.; Mobashery, S.; Piddock, L. J. V.; Projan, S.; Thomas, C. M.; Tomasz, A.; Tulkens, P. M.; Walsh, T. R.; Watson, J. D.; Witkowski, J.; Witte, W.; Wright, G.; Yeh, P.; Zgurskaya, H. I. Tackling Antibiotic Resistance. Nat. Rev. Microbiol. 2011, 9, 894-896.

8. Warnes, S. L.; Keevil, C. W. Mechanism of Copper Surface Toxicity in Vancomycin-Resistant Enterococci following Wet or Dry Surface Contact. Appl. Environ. Microbiol. 2011, 77, 6049-6059.

9. Wahlig, H.; Dingeldein, E. Antibiotics and Bone Cements - Experimental and Clinical Long-Term Observations. Acta Orthop. Scand. 1980, 51, 49-56.

10. Bridier, A.; Briandet, R.; Thomas, V.; Dubois-Brissonnet, F. Resistance of Bacterial Biofilms to Disinfectants: a Review. Biofouling 2011, 27, 1017-1032.

11. Madkour, A. E.; Tew, G. N. Perspective - Towards Self-Sterilizing Medical Devices: Controlling Infection. Polym. Int. 2008, 57, 6-10.

12. Takenaka, S.; Tonoki, T.; Taira, K.; Murakami, S.; Aoki, K. Adaptation of Pseudomonas sp Strain 7-6 to Quaternary Ammonium Compounds and Their Degradation via Dual Pathways. Appl. Environ. Microbiol. 2007, 73, 1797-1802.

13. Fullenkamp, D. E.; Rivera, J. G.; Gong, Y.; Lau, K. H. A.; He, L.; Varshney, R.; Messersmith, P. B. Mussel-Inspired Silver-Releasing Antibacterial Hydrogels. Biomaterials 2012, 33, 3783-3791.

14. Hasan, J.; Crawford, R. J.; Lvanova, E. P. Antibacterial Surfaces: The Quest for a new Generation of Biomaterials. Trends Biotechnol. 2013, 31, 31-40.

15. Ling, L. L.; Schneider, T.; Peoples, A. J.; Spoering, A. L.; Engels, I.; Conlon, B. P.; Mueller, A.; Schaeberle, T. F.; Hughes, D. E.; Epstein, S.; Jones, M.; Lazarides, L.; Steadman, V. A.; Cohen, D. R.; Felix, C. R.; Fetterman, K. A.; Millett, W. P.; Nitti, A. G.; Zullo, A. M.; Chen, C.; Lewis, K. A new Antibiotic Kills Pathogens Without Detectable Resistance. Nature 2015, 517, 455-459.

16. Ivanova, E. P.; Hasan, J.; Webb, H. K.; Truong, V. K.; Watson, G. S.; Watson, J. A.; Baulin, V. A.; Pogodin, S.; Wang, J. Y.; Tobin, M. J.; Löbbe, C.; Crawford, R. J. Natural Bactericidal Surfaces: Mechanical Rupture of Pseudomonas aeruginosa Cells by Cicada Wings. Small 2012, 8, 2489-2494.

17. Pogodin, S.; Hasan, J.; Baulin, V. A.; Webb, H. K.; Vi Khanh Truong; The Hong Phong Nguyen; Boshkovikj, V.; Fluke, C. J.; Watson, G. S.; Watson, J. A.; Crawford, R. J.; Ivanova, E. P. Biophysical Model of Bacterial Cell Interactions with Nanopatterned Cicada Wing Surfaces. Biophys. J. 2013, 104, 835-840.

18. Nowlin, K.; Boseman, A.; Covell, A.; LaJeunesse, D. Adhesion-Dependent Rupturing Ofsaccharomyces Cerevisiaeon Biological Antimicrobial Nanostructured Surfaces. J. R. Soc. Interface 2015, 12, 20140999.

19. Hasan, J.; Webb, H. K.; Vi Khanh Truong; Pogodin, S.; Baulin, V. A.; Watson, G. S.; Watson, J. A.; Crawford, R. J.; Ivanova, E. P. Selective Bactericidal Activity of Nanopatterned Superhydrophobic Cicada Psaltoda Claripennis Wing Surfaces. Appl. Microbiol. Biotechnol. 2013, 97, 9257-9262.

20. Xue, F.; Liu, J.; Guo, L.; Zhang, L.; Li, Q. Theoretical Study on the Bactericidal Nature of Nanopatterned Surfaces. J. Theor. Biol. 2015, 385, 1-7.

21. An, Y. H.; Friedman, R. J. Concise Review of Mechanisms of Bacterial Adhesion to Biomaterial Surfaces. J. Biomed. Mater. Res. 1998, 43, 338-348.

22. Freschauf, L. R.; McLane, J.; Sharma, H.; Khine, M. Shrink-Induced Superhydrophobic and Antibacterial Surfaces in Consumer Plastics. Plos One 2012, 7, e40987.

23. Crick, C. R.; Ismail, S.; Pratten, J.; Parkin, I. P. An Investigation into Bacterial Attachment to an Elastomeric Superhydrophobic Surface Prepared via Aerosol Assisted Deposition. Thin Solid Films 2011, 519, 3722-3727.

24. Alves, N. M.; Shi, J.; Oramas, E.; Santos, J. L.; Tomas, H.; Mano, J. F. Bioinspired Superhydrophobic Poly(L-Lactic Acid) Surfaces Control Bone Marrow Derived Cells Adhesion and Proliferation. J. Biomed. Mater. Res., Part A 2009, 91A, 480-488.

25. Bhushan, B.; Jung, Y. C. Natural And Biomimetic Artificial Surfaces for Superhydrophobicity, Self-Cleaning, Low Adhesion, and Drag Reduction. Prog. Mater. Sci. 2011, 56, 1-108.

26. Guo, Z.; Liu, W.; Su, B. Superhydrophobic surfaces: From Natural to Biomimetic to Functional. J. Colloid Interface Sci. 2011, 353, 335-355.

27. Zhang, X.; Wang, L.; Levanen, E. Superhydrophobic Surfaces for the Reduction of Bacterial Adhesion. RSC Adv. 2013, 3, 12003-12020.

28. Sun, T. L.; Feng, L.; Gao, X. F.; Jiang, L. Bioinspired Surfaces with Special Wettability. Acc. Chem. Res. 2005, 38, 644-652.

29. Watson, G. S.; Myhra, S.; Cribb, B. W.; Watson, J. A. Putative Functions and Functional Efficiency of Ordered Cuticular Nanoarrays on Insect Wings. Biophys. J. 2008, 94, 3352-3360.

30. Zhang, G.; Zhang, J.; Xie, G.; Liu, Z.; Shao, H. Cicada wings: A Stamp From Nature for Nanoimprint Lithography. Small 2006, 2, 1440-1443.

31. Hong, S.; Hwang, J.; Lee, H. Replication of Cicada Wing's Nano-Patterns by Hot Embossing and UV Nanoimprinting. Nanotechnology 2009, 20, 385303.

32. Sun, M.; Liang, A.; Zheng, Y.; Watson, G. S.; Watson, J. A. A Study of the Anti-Reflection Efficiency of Natural Nano-Arrays of Varying Sizes. Bioinspiration Biomimetics 2011, 6, 026003.

33. Sun, M.; Watson, G. S.; Zheng, Y.; Watson, J. A.; Liang, A. Wetting Properties on Nanostructured Surfaces of Cicada Wings. J. Exp. Biol. 2009, 212, 3148-3155.

34. Dellieu, L.; Sarrazin, M.; Simonis, P.; Deparis, O.; Vigneron, J. P. A two-in-one Superhydrophobic and Anti-Reflective Nanodevice in the Grey Cicada Cicada Orni (Hemiptera). J. Appl. Phys. 2014, 116, 024701.

35. Huang, Y.; Jen, Y.; Chen, L.; Chen, K.; Chattopadhyay, S. Design for Approaching Cicada-Wing Reflectance in Low- and High-Index Biomimetic Nano structures. ACS Nano 2015, 9, 301-311.

36. Strom, G.; Fredriksson, M.; Stenius, P. Kinetics of Oil Displacement from a Solid-Surface by an Aqueous-Solution. J. Colloid Interface Sci. 1990, 134, 117-121.

37. Strom, G.; Carlsson, G. Wettability of Kraft Pulps - Effect of Surface-Composition and Oxygen Plasma Treatment. J. Adhes. Sci. Technol. 1992, 6, 745-761.

38. Kaelble, D. H. Dispersion-Polar Surface Tension Properties of Organic Solids. J. Adhesion 1970, 2, 66-81.

39. Owens, D. K.; Wendt, R. C. Estimation of Surface Free Energy of Polymers. J. Appl. Polym. Sci. 1969, 13, 1741-1747.

40. Horcas, I.; Fernandez, R.; Gomez-Rodriguez, J. M.; Colchero, J.; Gomez-Herrero, J.; Baro, A. M. WSXM: A Software for Scanning Probe Microscopy and a Tool for Nanotechnology. Rev. Sci. Instrum. 2007, 78, 013705.

41. Zeiger, A. S.; Hinton, B.; Van Vliet, K. J. Why the Dish Makes a Difference: Quantitative Comparison of Polystyrene Culture Surfaces. Acta Biomater. 2013, 9, 7354-7361.

42. Campoccia, D.; Montanaro, L.; Arciola, C. R. A Review of the Biomaterials Technologies for Infection-Resistant Surfaces. Biomaterials 2013, 34, 8533-8554.

43. Cassie, A. B. D.; Baxter, S. Wettability of Porous Surfaces. Transactions of the Faraday Society 1944, 40, 546-550.

44. Becker, K. Detachment Studies on Microfouling in Natural Biofilms on Substrata with Different Surface Tensions. Int. Biodeterior. Biodegrad. 1998, 41, 93-100.

45. Harnett, E. M.; Alderman, J.; Wood, T. The Surface Energy of Various Biomaterials Coated with Adhesion Molecules Used in Cell Culture. Colloids Surf., B 2007, 55, 90-97.

46. Zhao, Q.; Wang, S.; Muller-Steinhagen, H. Tailored Surface Free Energy of Membrane Diffusers to Minimize Microbial Adhesion. Appl. Surf. Sci. 2004, 230, 371-378.

47. Pereni, C. I.; Zhao, Q.; Liu, Y.; Abel, E. Surface Free Energy Effect on Bacterial Retention. Colloids Surf., B 2006, 48, 143-147.

TOC figure